AJNR

High-Sensitivity Coil Array for Head and Neck Imaging: Technical Note

Roland G. Henry, Nancy J. Fischbein, William P. Dillon, Daniel B. Vigneron and Sarah J. Nelson

High-Sensitivity Coil Array for Head and Neck Imaging: Technical Note

Roland G. Henry, Nancy J. Fischbein, William P. Dillon, Daniel B. Vigneron, and Sarah J. Nelson

Summary: The purpose of this study was to develop coils for MR imaging of the head and neck region, with the aim of improving sensitivity and coverage. A head and neck phased array coil was constructed and compared with volume and temporomandibular joint surface coils for sensitivity and coverage in phantom studies. An algorithm was implemented to correct for the nonuniformity in the surface coil reception profile. Its application to high-resolution T2-weighted imaging in healthy volunteers was investigated.

An improved signal-to-noise ratio (SNR) for imaging of the head and neck is needed for high-resolution anatomic imaging and other MR imaging techniques, such as perfusion and spectroscopic imaging. The purpose of this study was to develop coils for MR imaging of the head and neck region, with the aim of improving sensitivity and coverage. Imaging of the neck region usually is accomplished with surface coils, which have high sensitivity, or volume coils, which encircle the region of interest. Surface coils provide a higher SNR (1–7), but they have limited coverage relative to their size and rapidly changing reception sensitivity. Volume coils used in head and neck MR imaging provide good uniformity and coverage of this region, but they have relatively poor SNRs. The ideal head and neck coil combines the coverage and uniformity of the volume coils with the higher SNR of the surface coils. To meet these criteria, we constructed an array of surface coils with both high sensitivity and good coverage. Although the designs of many coils are influenced by uniformity considerations, the head and neck array was designed to maximize sensitivity and coverage, and a low-pass filter algorithm (1) was used to correct for the lack of reception uniformity.

Description of Coil

Coil Construction

We constructed four coils by etching 7 × 8-cm hexagonal loops from a flexible circuit board (Py-

rolux; DuPont Instruments, Wilmington, DE). With a network analyzer (Hewlett Packard), which measures the frequency versus the Q value for a linear circuit, the coils were individually tuned to the MR carrier frequency by adjusting capacitor values. Diode trap circuits used to detune the surface coils during excitation with the body coil were constructed for each of the surface coils, and the input impedances were matched to 50 ohms.

Two of the 7 × 8-cm hexagonal coils were slightly overlapped to minimize the coupling between the coils, as measured with the network analyzer. The final positions corresponded to 20-dB decoupling between the coils. The pair of overlapped coils was mounted on a plastic frame. The head and neck phased array coil comprised two such pairs placed on the patient's left and right to cover the nasopharynx to the shoulder with the long dimension of the two-coil configuration.

The lateral coils were slightly overlapped (Fig 1) to minimize the mutual inductance of the coils; the loaded decoupling was measured at 20 dB in the laboratory. Phantom and volunteer studies in which the signals were individually examined indicated little coupling between contralateral and overlapping coils of the array. This prototype coil is not commercially available.

SNR Measurements

The SNR of the head and neck phased array coil was compared with that of two volume neck coils in current clinical use, the Medrad Anterior Neck Coil and the Medical Advances Neurovascular Coil. Axial sections of a cylindrical water phantom, 14 cm in diameter and 18 cm long, were acquired with each coil, by using a proton density–weighted fast spin-echo (FSE) sequence. For each coil, the average signal intensities were determined as a function of transaxial position for two axial regions: 5-cm-diameter circular regions at the center of the axial sections and 3-cm-diameter circular regions centered 2.5 cm from the surface of the phantom. The noise was assumed to be uniform for the entire volume and was obtained from the standard deviation of pixel values from regions outside the phantom where the signal is expected to originate from noise only.

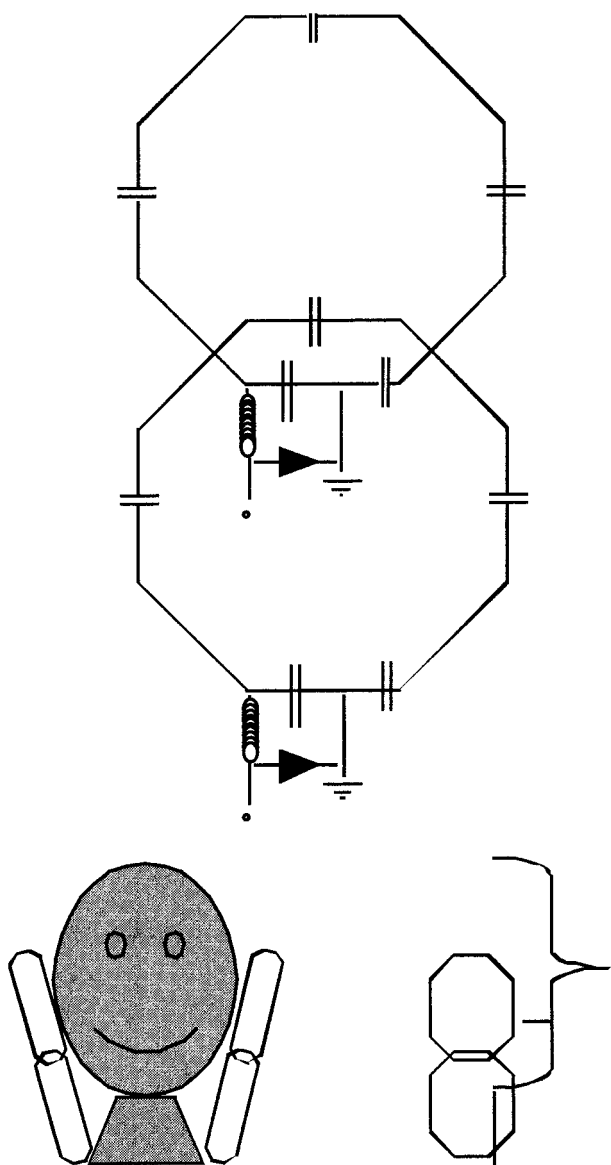The SNR of the head and neck phased array coil (Fig 2) was four to five times higher near the sur-

FIG 1.   Schematic drawings of overlapping 7 × 8-cm octagonal elements used to construct the head and neck surface coil array.

FIG 2.   Graph shows the relative SNR in units of the average SNR from the volume coils for the head and neck surface coil array (*smooth lines*); temporomandibular joint phased array coils (*dotted-and-dashed line*); and volume head and neck coils, which are the anterior neck coil (*dashed line, ANC*) and quadrature neck coil (*dotted line, QNC*). The SNR for the head and neck phased array and temporomandibular joint phased array were calculated from a region near the surface of the phantom (*HNPA Edge* and *TJMPA Edge,* respectively) and also from the center of the phantom for the head and neck phased array (*HNPA Center*). The SNR for the volume coils were calculated from regions near the center of the phantom for best uniformity.

FIG 3.   Graphs shows the right-to-left SNR for the head and neck surface coil array in units of the average SNR from the volume coils. The head and neck surface coil array has a transaxial SNR more than four times higher than that of the volume coil as far as 2 cm inside the phantom at the center of the coils (125 mm in Fig 2).

face and was comparable with that of the volume coils at the center of the phantom. The temporomandibular joint phased array coil had an SNR that was a little higher than that of the head and neck phased array coil at the center of the coil, but the head and neck phased array coil covered approximately 50 mm more than did the temporomandibular joint phased array coil, with high sensitivity (Fig 2). The head and neck phased array coil had an SNR that was comparable or better than that of the volume coils for a transaxial range of approximately 180 mm; its coverage was similar to that of the volume coils (Fig 2). The axial SNR profile from the phantom studies (Fig 3) also suggested that the head and neck phased array SNR is higher at the center in vivo because typical necks are 11.0–11.5 cm in diameter and therefore smaller than the 14-cm-diameter phantom.
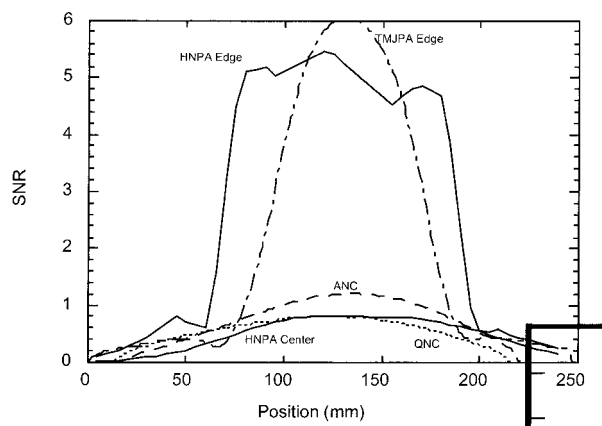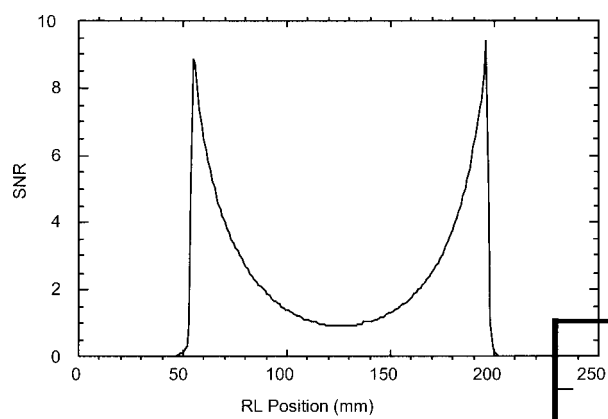
Coil Intensity Profile Correction

The coil reception profile intensity correction uses a gaussian low-pass filter of the image as an approximation to the coil sensitivity map (1). Because of the lack of signal at and near the object edge, the low-pass filter approximate map is incorrectly calculated to be lower than it should be, resulting in undercorrection of the image at these edges. This problem was solved by using an edge-detection algorithm first to detect the head and neck–to-air interface. The edge-completion method (1) was used to correct this problem. This method was used to identify the region on the edge of the object where the signal intensity drops off because
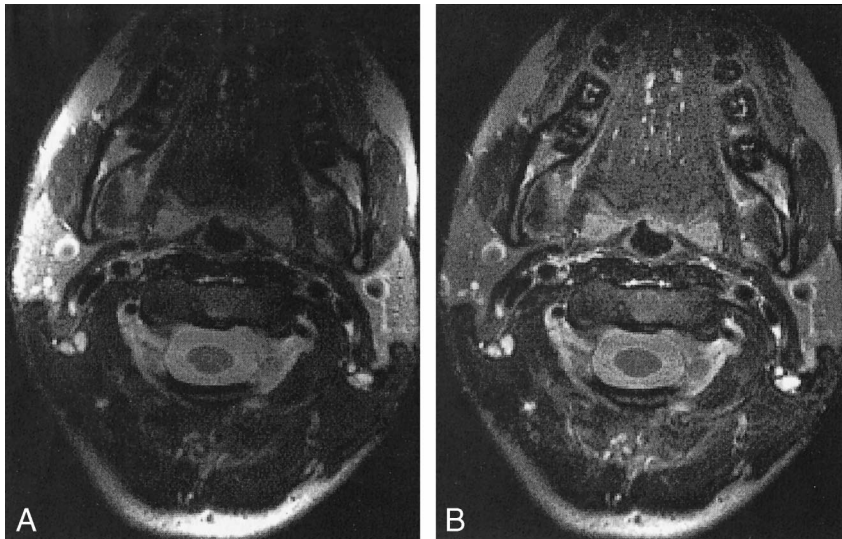
FIG 4.   2D T2-weighted FSE MR images (4-mm section, 16-cm FOV, 256 × 256 matrix) of a healthy volunteer's neck. A bright region at the posterior edge is the result of inadequate edge completion.
   A, Uncorrected image.
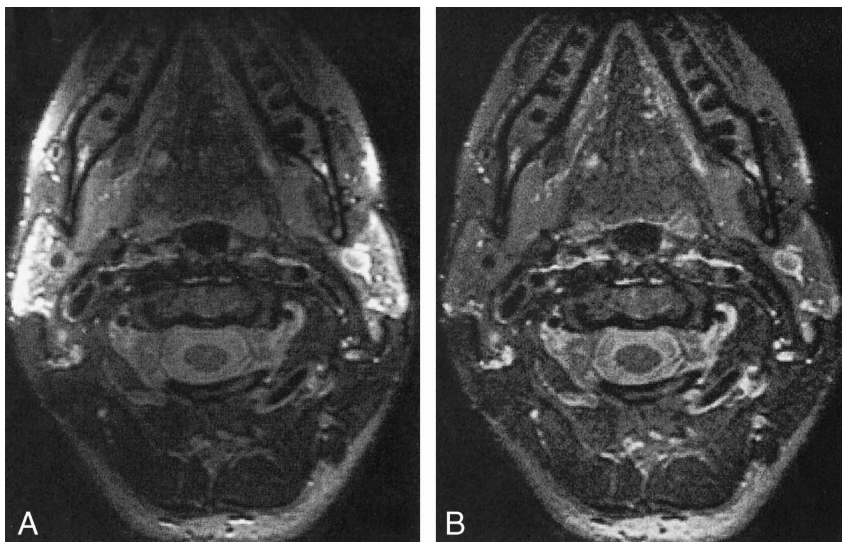   *B,* Images corrected with a low-pass filter algorithm.

FIG 5.   3D T2-weighted FSE MR images (1-mm section, 18-cm FOV, 256 × 192 matrix) of a healthy volunteer's neck. As in Figure 4, the edge completion at the posterior edge of the images is suboptimal.
   A, Uncorrected image.
   B, Image corrected with a low-pass filter algorithm.

of partial volume effects with the air and replace the pixels outside of this edge with values with the edge pixel values. The edge-completed image was then used to generate the approximate coil sensitivity map.

Images from phantom studies with the head and neck phased array coil were successfully corrected by using this edge-completed low-pass filtered algorithm. Uncorrected and corrected images of a healthy volunteer's neck were acquired by using T2-weighted 2D and 3D FSE pulse sequences (Figs 4 and 5). A disadvantage of the low-pass filter correction map method originates from image structure remaining in the field map approximation. For example, the object edges and large high-contrast objects within the image, such as CSF around the spinal cord, contribute to the low-pass filter that is used to approximate the slowly varying coil reception profile.

High-Resolution 2D and 3D FSE Imaging

FSE imaging has enabled high-resolution T2-weighted imaging by reducing acquisition time while allowing averaging over multiple acquisitions within a reasonable imaging time. Using the head and neck phased array coil, we optimized 2D and 3D FSE imaging of the head and neck region. Averaging over four acquisitions with a 2D FSE sequence was performed in volunteers, with the following parameters: echo train length, 16; receiver bandwidth, 16 kHz; no phase wrapping; field of view (FOV), 12–16 cm; acquisition size, 256 × 256; section thickness, 2–4 mm; and concatenated inferior, superior, and chemical fat saturation. A 3D FSE sequence was used to obtain high-resolution T2-weighted images in 10.5 min, with the following parameters: echo train length, 16; eight locations per slab; FOV, 18 cm; acquisition size, 256 × 192; number of excitations, one; and inferior,

FIG 6. Comparison of corrected FSE MR images obtained with the head and neck phased array coil.

A, 2D images (256 × 256 matrix, 4-mm section, 30 images, 16 [axial] × 15 [trans-axial]-cm FOV).

B, 3D images (256 × 192 matrix, 1.5-mm section, 18 [axial] × 18 [transaxial]-cm FOV). The SNR is slightly worse with the 3D sequence, but resolution and coverage are better in the same imaging time.
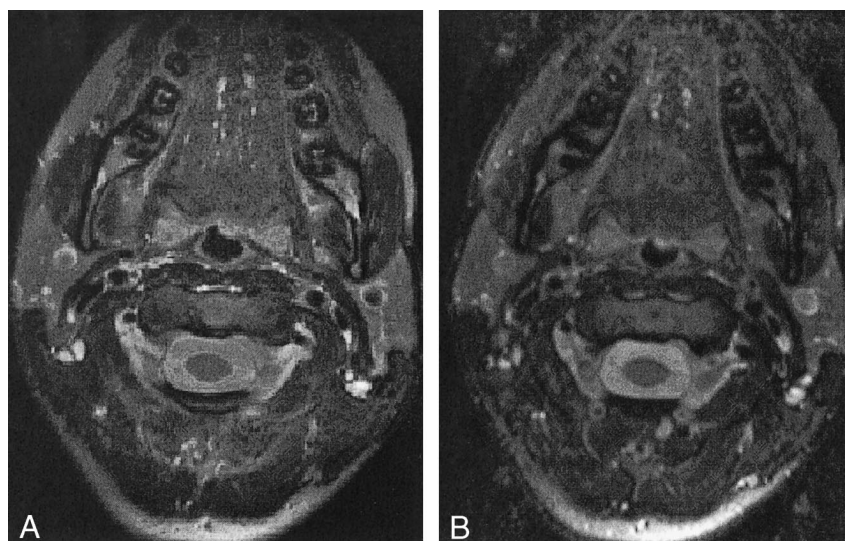
superior, and chemical fat saturation. All imaging was performed by using a 1.5-T magnet (Echospeed; GE Medical Systems, Milwaukee, WI).

Figure 6 shows a comparison of 2D and 3D images acquired with the head and neck phased array coil and corrected for the coil reception. A disadvantage of the 2D FSE sequence was the limited number of images in the section direction, namely, 30 images in 10 min. Three-dimensional FSE overcame this limitation and provided 120 images in the section direction, with an imaging time of 10.5 min. Furthermore, the SNR of the 3D sequence improved in the 3D acquisition mode. Reformations of 3D FSE axial data with almost isotropic voxels are shown in Figure 7.

A disadvantage of the 3D sequence is artifact due to CSF and vascular flow. Although vascular flow was also a problem for 2D FSE imaging, the CSF flow did not produce as much of an artifact because of the short imaging time for each section compared with the CSF flow rate. For 3D acquisition, many more phase encodes (eight to 10 times more for our sequence) were used to form a single section. For instance, a 2D section is acquired within 1 TR, compared with 10 TRs for a 3D section. Hence, unprepared CSF may flow into the encoding volume during acquisition, producing artifacts. For 3D acquisition, the in-plane resolution was limited by the need to cover the entire anatomy to avoid phase wrapping, because the ''no phase wrap'' option was not compatible with 3D acquisition.

Figure 8 shows a comparison of the head and neck phased array coil and the anterior neck coil on a 2D T2-weighted image in a healthy volunteer. The axial images are slightly rotated with respect to each other, but the SNR advantage was evident with the head and neck phased array coil. Although the volume coils are fairly uniform, some intensity variation was evident in Figure 8B.

Discussion

We constructed a surface coil array for MR imaging of the entire face and neck region. This coil provides sensitivity that is higher than that of volume coils over a comparable region, but it has intensity variation because of the inhomogeneous reception profile. The increased SNR with good coverage may improve determination of the extent of disease compared with evaluation with conventional MR imaging, and it should provide sufficient SNR for functional studies such as dynamic perfusion or spectroscopic studies of the entire potentially diseased region.

The low-pass filter correction algorithm corrects the inhomogeneous sensitivity of the surface coil arrays well. The correction of surface coil images has also been achieved by using analytic and phantom-based approaches. Phantom-based methods are used to correlate images in phantoms and humans to correct for inhomogeneous coil sensitivity. This method is complicated by the need to make the correlation and the fact that the intensities on phantom images may easily differ from those on human images because of slightly different coil placement. The analytic method uses a calculated coil sensitivity map to make the correction. However, this method generally does not include signal changes due to coil interactions, and the coil placement has to be known in 3D. The signal inhomogeneity of the images acquired with the head and neck phased array coil does not present a problem for the analysis of perfusion data, because with most techniques, image division cancels this effect. Spectral data also can be corrected with the low-pass filter technique by using the approximate coil map obtained from anatomic images.

In the evaluation of tumors in the head and neck at conventional MR imaging, FSE T2-weighted imaging has been found to provide better tumor conspicuity in a shorter imaging time, compared with traditional spin-echo T2-weighted imaging (8, 9). Fat-suppressed contrast-enhanced T1-weighted imaging also adds information in certain situations (10, 11). For T2-weighted acquisitions, volume coils generally require a section thickness of at
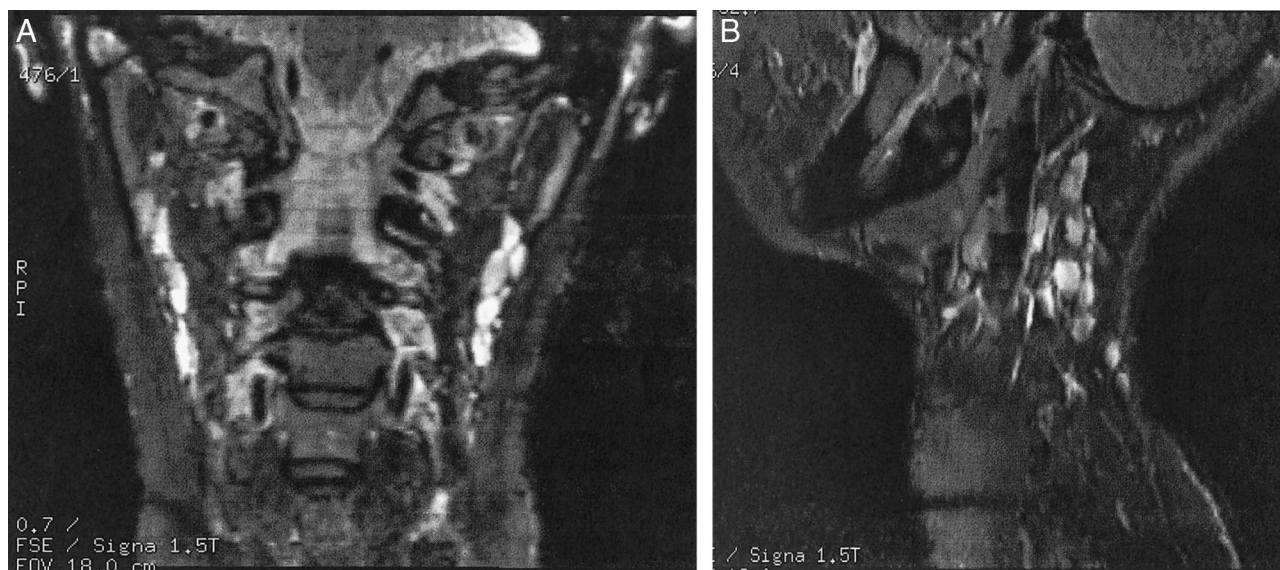
FIG 7. *A* and *B*, Reformations from corrected axial T2-weighted 3D FSE MR data (1.0-mm section thickness, 18 cm FOV, 256 × 192 matrix). The thin sections allow for good-quality reformations, and even small lymph nodes are clearly depicted.
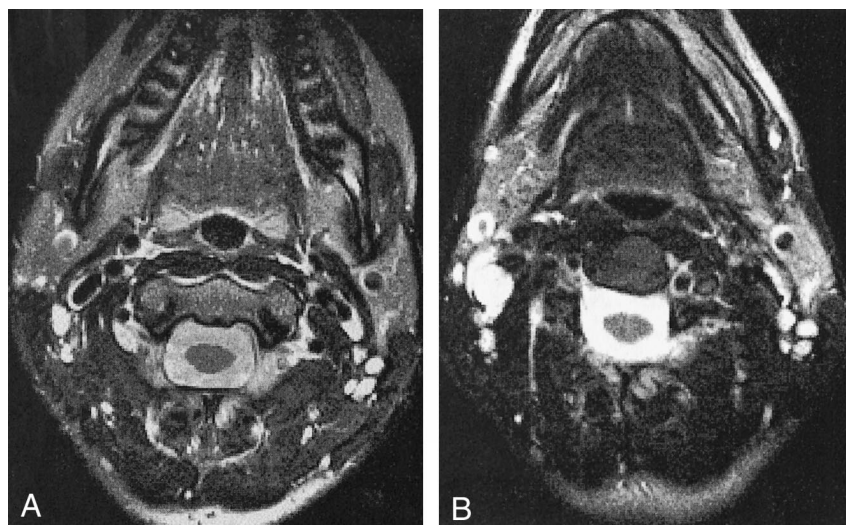

FIG 8. Axial 2D FSE MR images (4-mm section, 16-cm FOV, 256 × 256 matrix).
A, Images acquired with the head and neck phased array coil. Compared with the anterior neck coil, the head and neck phased array has a higher SNR that results in sharper images with better definition of small structures, such as cervical lymph nodes.
B, Images acquired with the anterior neck coil.

least 4 mm to ensure adequate SNR. This section profile reduces the ability to evaluate small (2–5 mm) neck nodes or to determine the involvement of crucial head and neck structures, such as the carotid artery near the adjacent tumor. A head and neck surface coil array can provide improved SNR and resolution along with clinically acceptable coverage for T2-weighted images.

A 3D FSE pulse sequence can be used to obtain a high-resolution (1.0 × 0.7 × 0.9 mm) T2-weighted volume in 10.5 min. Although 2D FSE imaging may also yield high-resolution images with good SNR in a short imaging time, the limitation in the number of sections in the series forces a compromise between section thickness and section FOV. Although flow artifacts are more pronounced on the 3D FSE images, the intensity-corrected 3D data can be reformatted to produce high-quality images in any cartesian and oblique orientation.

Other anatomic imaging sequences also should benefit from the improved SNR that surface coil array provides. For example, higher resolution can be obtained on T1-weighted images than was previously possible with volume coils; this feature is especially useful for depicting contrast enhancement in small neck nodes, subtle tumor infiltration into adjacent structures, and residual disease. Functional techniques, such as quantitative dynamic perfusion imaging and proton spectroscopic imaging, tend to have poor SNR. The improved SNR with the head and neck phased array coil can allow use of these techniques in the study of primary tumors and neck node disease, as well as in the serial study of responses to treatment.

Conclusion

We constructed a head and neck phased array coil that has superior sensitivity compared with

volume coils and better coverage than temporo-mandibular joint coils. The higher sensitivity of the head and neck phased array has enabled high-resolution T2-weighted imaging and should improve quantitative perfusion and proton spectroscopic imaging studies in the head and neck region.

References

1. Wald LL, Carvajal L, Moyher SE, et al. **Phased array detectors and an automated intensity-correction algorithm for high-resolution MR imaging of the human brain.** *Magn Reson Med* 1995;34:433–439
2. Moyher SE, Vigneron DB, Nelson SJ. **Surface coil MR imaging of the human brain with an analytical reception profile correction.** *J Magn Reson Imaging* 1995;5:139–144
3. Hayes CE, Hattes N, Roemer PB. **Volume imaging with MR phased arrays.** *Magn Reson Med* 1991;18:309–319
4. Hayes CE, Tsuruda JS, Mathis CM. **Temporal lobes: surface MR coil phased-array imaging.** *Radiology* 1993;189:918–920
5. Roemer PB, Edelstein WA, Hayes CE, Souza SP, Mueller OM. **The NMR phased array.** *Magn Reson Med* 1990;16:192–225
6. Hayes CE, Roemer PB. **Noise correlations in data simultaneously acquired from multiple surface coil arrays.** *Magn Reson Med* 1990;16:181–191
7. Hayes CE, Dietz MJ, King BF, Ehman RL. **Pelvic imaging with phased-array coils: quantitative assessment of signal-to-noise ratio improvement.** *J Magn Reson Imaging* 1992;2:321–326
8. Zoarski GH, Mackey JK, Yashimi A, et al. **Head and neck: initial clinical experience with fast spin-echo imaging.** *Radiology* 1993;188:323–327
9. Fulbright R, Panush D, Sze G, Smith RC, Constable RT. **MR of the head and neck: comparison of fast spin-echo and conventional spin-echo sequences.** *AJNR Am J Neuroradiol* 1994;15:767–773
10. Ross MR, Schomer DF, Chappell P, Enzmann DR. **MR imaging of head and neck tumors: comparison of T1-weighted contrast-enhanced fat-suppressed images with conventional T2-weighted and fast spin-echo T2-weighted images.** *AJR Am J Roentgenol* 1994;163:173–178
11. Dubin MD, Teresi LM, Bradley WG Jr, et al. **Conspicuity of tumors of the head and neck on fat-suppressed MR images: T2-weighted fast-spin-echo versus contrast-enhanced T1-weighted conventional spin-echo sequences.** *AJR Am J Roentgenol* 1995;164:1213–1221